This is an *Accepted Manuscript*, which has been through the Royal Society of Chemistry peer review process and has been accepted for publication.

Accepted Manuscripts are published online shortly after acceptance, before technical editing, formatting and proof reading. Using this free service, authors can make their results available to the community, in citable form, before we publish the edited article. We will replace this *Accepted Manuscript* with the edited and formatted *Advance Article* as soon as it is available.

You can find more information about *Accepted Manuscripts* in the **Information for Authors**.

Please note that technical editing may introduce minor changes to the text and/or graphics, which may alter content. The journal's standard **Terms & Conditions** and the **Ethical guidelines** still apply. In no event shall the Royal Society of Chemistry be held responsible for any errors or omissions in this *Accepted Manuscript* or any consequences arising from the use of any information it contains.

ChemComm

COMMUNICATION

High-performance nanoporous Si/Al₂O₃ foam lithium-ion battery anode fabricated by selective chemical etching of Al-Si alloy and subsequent thermal oxidation

Gaeun Hwang, Hyungmin Park, Taesoo Bok, Sinho Choi, Sungjun Lee, Inchan Hwang, Nam-Soon Choi, Kwanyong Seo and Soojin Park*

Nanostructured micrometer-sized Al-Si particles are synthesized via a facile selective etching process of Al-Si alloy powder. Subsequent thin Al₂O₃ layers are introduced on the Si foam surface via a selective thermal wet oxidation process of etched Al-Si particles. The resulting Si/Al₂O₃ foam anodes exhibit outstanding cycling stability (capacity retention of 78% after 300 cycles at C/5 rate) and excellent rate capability.

Silicon (Si) is one of the most attractive anode materials for rechargeable lithium-ion batteries (LIBs) owing to its abundance in nature, low cost, relatively low working potential (<0.4 versus Li/Li⁺) and high theoretical capacity (3579 mA h g⁻¹ with composition of $Li_{15}Si_4$ at room temperature).[1, 2] However, the large volume change of Si (>300%) during the Li insertion/extraction process gives rise to pulverization of Si electrodes, the formation of an unstable thick solid-electrolyte-interface (SEI) layer, and acceleration of electrolyte depletion, resulting in serious capacity fading. These problems hinder commercial use of Si anode materials in LIBs.

In order to overcome these problems, numerous strategies have been developed to release the large strain and stress that occur during the cycling of Si anodes, by introducing concepts of nanostructuring, such as nanoparticles,[3] nanowires,[4] nanotubes[5] and nanocomposites.[6,7] For example, Chan et al. demonstrated that Si nanowire can prevent the initiation of fractures because the small nanowire diameter can endure a large volume change.[7] Zhou et al.[8] and Jiang et al.[9] proposed a simple and cost-effective method to synthesize nanostructured porous Si by hydrochloric acid etching of Al-Si alloy particles. They showed that the nanostructured Si is effective at improving electrochemical performances because the reduced dimension both increases the rate of lithium insertion/extraction owing to the short distance for Li-ion transport within the particles and also enhances the electron transport within the particles. However, a large portion of polymeric binders was used and initial coulombic efficiency (ICE) was low due to a side reaction of the Al-Si electrode and electrolyte.

Introducing protection layers on the surface of various structured Si particles has been suggested as another effective method to reduce the side reaction and to form stable SEI layers on the Si surface. For example, carbon,[10] metal,[11] metal oxide,[12] metal silicide,[13, 14] and conducting polymer coating layers[15] have been introduced on the Si surface to maintain the original Si structure and to enhance electrical conductivity. Among these materials, Al₂O₃ deposited by the atomic layer deposition (ALD) method has been studied as a protection layer on the Si surface.[16, 17] It showed significantly improved cycling performance due to the suppression of the side reaction between Si and electrolyte by the thin Al₂O₃ layer. However, the ALD process is not a cost-effective way for large scale production of Si-based materials.

Herein, we demonstrate a simple and cost-effective synthesis of micron-scale nanostructured Si/Al₂O₃ foam particles from Al-Si alloy by combining chemical etching with a selective thermal oxidation process. The amount of Al is controlled by the etching time and subsequent preferential thermal oxidation of Al layers leads to the formation of Si/Al₂O₃ foam. As-synthesized Si/Al₂O₃ foam is tested as an LIB anode. It exhibits outstanding cycling stability (capacity retention of 78% after 300 cycles at C/5 rate), excellent rate capability, and suppressed volume expansion after long-term cycling.

Micro-scale nanostructured Al-Si foam was prepared by acid etching of Al-Si alloy powder (Fig. 1a). The hydrochloric acid (HCl) etchant preferentially attacks Al, resulting in the formation of a foam-type Si structure (including a small amount of remaining Al depending on the etching conditions) without a serious collapse. The following equation shows the etching reaction with Al and HCl.

$$2Al\ (s) + 6HCl\ (aq) \rightarrow 2AlCl_3\ (aq) + 3H_2\uparrow$$
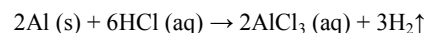
A scanning electron microscopy (SEM) image of pristine Al-Si powder shows that the particle diameters are in the range of 1-6 μm (Fig. 1b). When the Al-Si particles (13 g) were etched in 3M HCl at room temperature for 30 min, an Al-Si foam-like structure with a Si frame of 50-100 nm was obtained (Fig. 1c). Microstructures of the

pristine (Fig. 1d) and the chemically etched Al-Si particles (Fig. 1e) were investigated by X-ray diffraction (XRD) patterns. After chemical etching, the peak intensity of Al was significantly decreased (around 5 times lower than that of the pristine sample). To characterize the amount of Al and Si of both samples, energy-dispersive X-ray spectroscopy (EDS) was employed. The pristine Al-Si powders contain 85wt% of Al and 11 wt% of Si, while the etched sample shows 21wt% Al and 67 wt% Si because of a selective etching of Al parts (ESI, Fig. S1 and Table S1). Al contents ranging from 60 wt% to 4wt% can be easily tuned by controlling the etching time from 15 to 60 min at the same etching condition (ESI, Table S1). Among various Al-Si foam particles, we selected the 30 min-etched sample as a model system for making Si/Al_2O_3 foam particles, because 10 min-etched sample were partially etched and 60 min-etched particle were seriously etched away with a destruction of the original structure (ESI, Fig. S2).
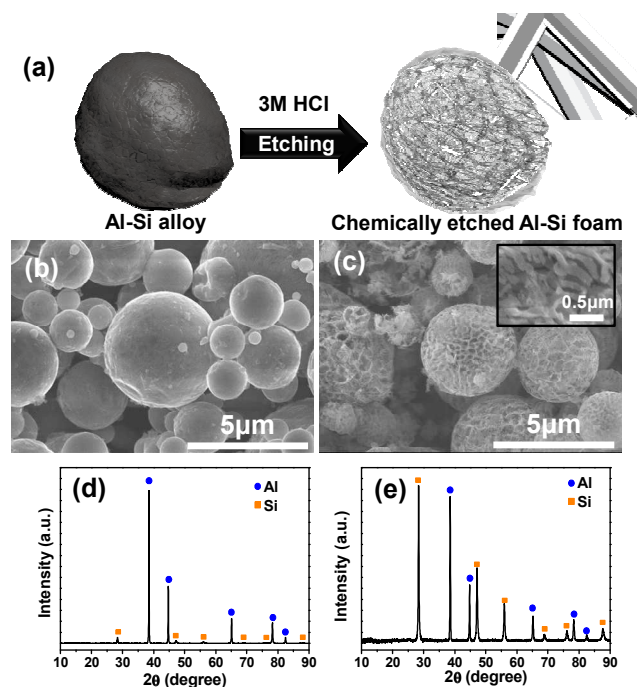
Fig. 1 (a) Schematic illustration showing synthetic process of Al-Si foam-like particles. SEM images of (b) pristine Al-Si alloy and (c) chemically etched Al-Si powder. XRD patterns of (d) Al-Si alloy and (e) chemically etched Al-Si powder.

Fig. 2a illustrates the synthesis of Si/Al_2O_3 foam particles fabricated by the selective oxidation of Al by a thermal oxidation process performed at 600 ^{o}C with controlled water vapour. High-angle annular dark-field scanning transmission electron microscopy (HAADF-STEM) and the corresponding EDS mapping images of chemically etched Al-Si and the thermally oxidized (10 min) sample show that thin Al_2O_3 layers are coated on the Si frame in the outer shell, while Al_2O_3 particles of 500-600 nm diameter are located in the core of the Si/Al_2O_3 foam as major components (Fig. 2b). This can be explained as follows: the diffusion rate of chemical etchant gradually decreases from surface to core, so that a large amount of Al is etched out of the outer shell, but most of the Al is still intact in the core regions.

To convert residual Al to Al_2O_3, a thermal oxidation process of chemically etched (30 min) Al-Si powder was performed at 600 ^{o}C for three different periods of time. The etched Al-Si powders were exposed to water vapour at 600 ^{o}C for 10, 30, and 60 min to control the thickness of the Al_2O_3 layers. It should be noted that the Si species was not easily oxidized at 600 °C even in a wet atmosphere.[18, 19] After the oxidation process, the amount of oxygen was increased for all three samples, while the original foam-like structure was maintained because thermal oxidation was performed at well below the melting temperature of Al (T_m = 660.32 °C) (Fig. 2c and Fig. S3). Also, XRD patterns of the chemically etched and thermally oxidized samples show that the peak intensity of pure Al is gradually decreased with increasing oxidation time (Fig. 2d). However, XRD patterns of newly developed Al_2O_3 are not clearly seen, because thermal oxidation of Al at low temperature leads to the formation of amorphous Al_2O_3.[20, 21] To investigate oxidation rate of Si and Al, we used pure Si nanoparticles (average diameter of 100 nm) and pure Al particles (3 μm) in the same thermal oxidation condition. The SiO_2 layers on the Si surface were grown with thickness of ~3 nm after thermal oxidation for 60 min, while amorphous Al_2O_3 layers of ~6 nm were formed on the Al surface at 600 ^{o}C for 10 min (ESI, Fig. S4). As another control experiment, thermal oxidation process of Al particles was monitored by XRD patterns. When the Al particles were thermally oxidized at 600 ^{o}C for 10 min, 30 min, and 60 min, Al_2O_3 layers of 20%, 25%, and 35% were formed, respectively (ESI, Fig. S5). Furthermore, we investigated the Brunauer–Emmett–Teller (BET) surface area of etched Al-Si particle (29.2 m^2 g^{-1}) and thermally oxidized sample (10 min, 22.1 m^2 g^{-1}) (ESI, Fig. S6).

From these results, we can say that the Al_2O_3 layers were successfully introduced on the Si surface with controlled thickness. Since the Si/Al_2O_3 foam particles have many void spaces which can act as buffer layers for the large volume change of Si electrodes, and provide Al_2O_3 protecting layers which can reduce the side reaction between Si and electrolyte, they would be useful as LIB anodes.

Electrochemical performances of chemically etched (30 min) Al-Si and thermally oxidized Si/Al_2O_3 foam electrodes were tested in the potential range of 0.005-2.0 V (versus Li/Li$^+$) in a coin-type half cell (2016R). Fig. 3a shows the first cycle voltage profiles of the etched Al-Si and thermally oxidized Si electrodes obtained at C/20 rate. The etched Si-Al electrodes showed a high charge capacity of 1953 mA h g^{-1} in the first cycle, because both Si and Al (theoretical capacity of 993 mA h g^{-1} with composition of LiAl)[22] contribute to the specific capacity. In contrast, the Si/Al_2O_3 electrodes thermally oxidized for 10, 30, and 60 min exhibit 1384 (ICE = 83.1%), 1047 (ICE = 82.6%), and 843 mA h g^{-1} (ICE = 82.1%), respectively. This is attributed to the increase of inactive Al_2O_3 contents in the Si/Al_2O_3 particles at the increased oxidation times. Also, the ICE value with increasing oxidation time gradually decreases due to the insulating property of Al_2O_3 layers.

All Si/Al_2O_3 electrodes showed a lower specific capacity compared to the etched Al-Si electrodes. However, the Si/Al_2O_3 electrodes exhibited outstanding cycling stability at a rate of C/5 until 150 cycles (Fig. 3b). The etched Al-Si electrode showed fast capacity fading and a poor coulombic efficiency per cycle. It may be attributed to serious side reactions of Si/electrolyte and Al/electrolyte.[22] On the contrary, the Si/Al_2O_3 electrodes oxidized for 10, 30, and 60 min exhibit 854, 683, and 628 mA h g^{-1} after 150 cycles, respectively, which correspond to capacity retentions of 79%,

84%, and 93% compared to initial capacity. In particular, the 10 min-oxidized Si/Al$_2$O$_3$ electrode showed excellent long-term cycling stability (capacity retention of 78% after 300 cycles at C/5 rate) (Fig. 3c).
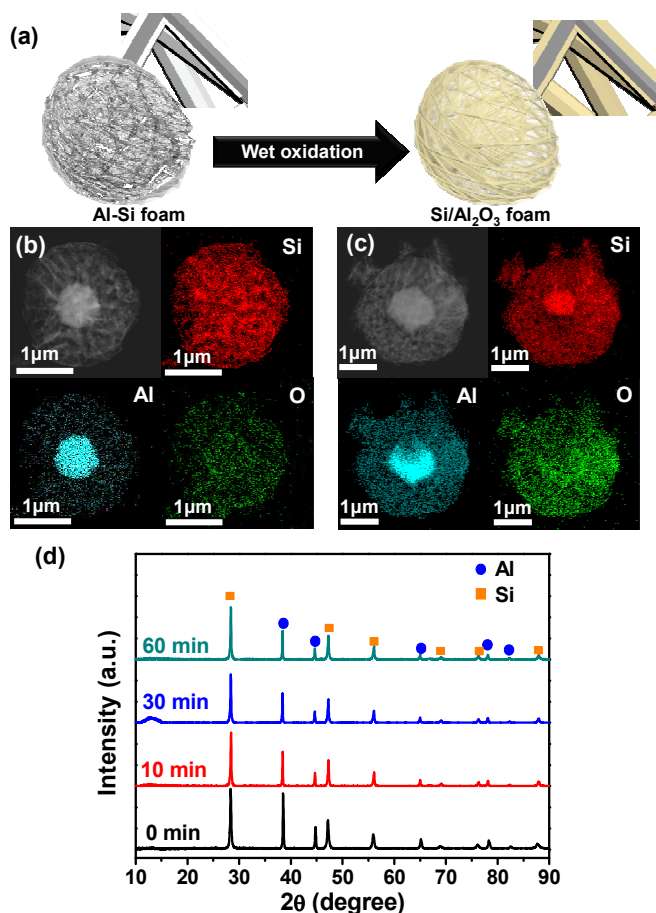
Fig. 2 (a) Schematic illustration showing thermal oxidation process of chemically etched Al-Si particles. HAADF-STEM and the corresponding EDS mapping images of (b) etched Al-Si powder and (c) thermally oxidized (10 min) Al-Si powder. (d) XRD patterns of chemically etched Al-Si and three different thermally oxidized Al-Si powders.

The effect of the Al$_2$O$_3$ layer on the electrochemical property can also be identified by electrochemical impedance spectroscopy (EIS) analyses of first-cycled and 120-cycled electrodes (ESI, Fig. S7). EIS spectra of all electrodes did not show any semicircles due to a thin SEI layer and low charge transfer resistance at the first cycle. However, after 120 cycles, the etched Al-Si electrode showed larger SEI and charge transfer resistance than the other oxidized Si/Al$_2$O$_3$ electrodes. This result indicates that the Al$_2$O$_3$ protective layer promotes the formation of a stable SEI layer on the Si surface.

Moreover, we tested the rate capabilities of the etched Al-Si and the oxidized Si/Al$_2$O$_3$ electrodes with various delithiation rates (from C/5 to 10C) at a fixed lithiation rate of C/5. The etched Al-Si electrode showed a large capacity drop from 1525 mA h g^{-1} at 0.2C to 269 mA h g^{-1} at 10C and did not recover initial specific capacity after 70 cycles. In contrast, thermally oxidized Si/Al$_2$O$_3$ electrodes exhibited excellent rate capabilities (10 min: capacity of 79% at 7C, 30 min: capacity of 82% at 7C, and 60 min: capacity of 85% at 7C, compared to capacity at C/5 rate). Also, these electrodes recovered their capacity to the initial specific capacity after 70 cycles. In

addition to delithiation rate capability, lithiation rate capabilities were tested for all Si-based electrodes (ESI, Fig. S8). The specific capacity of the etched Al-Si electrode quickly decayed at 3C rate, while the oxidized electrodes (10 min and 30 min) still showed a high capacity of ~400 mA h g^{-1} at 3C rate. From the XRD shown in Fig. 2d, we estimated the remaining Al contents. Samples oxidized for 10 min, 30 min, and 60 min still contained the remaining Al contents of 11%, 10%, and 9%, respectively, compared to the etched Al-Si particles. However, most Al thin layers except for the core region are converted to amorphous Al$_2$O$_3$ layers. Since the Si/Al$_2$O$_3$ foam with a thin Al$_2$O$_3$ layer has sponge-like structure in the shell region (except for the Al-rich core region), rate capability of this electrode is not affected too much depending on the thermal oxidation time. These results indicate that thin Al$_2$O$_3$ protecting layers prevent side reaction of the nano-sized Si frame in the foam and allow fast transport of lithium ions.
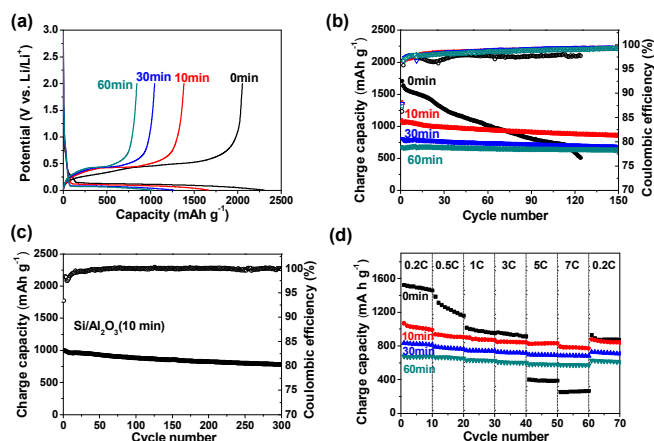
Fig. 3 Electrochemical performances of etched Al-Si and thermally oxidized (10, 30, and 60 min) Si/Al$_2$O$_3$ electrodes. (a) First cycle voltage profiles obtained at C/20 rate and (b) cycling performances at C/5 rate for four Si-based electrodes. (c) Long-term cycling stability of thermally oxidized (10 min) Si/Al$_2$O$_3$ electrode. (d) Rate capabilities of four Si-based electrodes obtained in the range of C/5-10C (lithiation rate was fixed at C/5).

Volume expansion of Si-based electrodes during repeated cycles is one of the critical issues. After the long-term cycling test of the etched Al-Si and the oxidized Si/Al$_2$O$_3$ electrodes, volume expansion of the electrodes was measured (ESI, Fig. S9). As expected, all oxidized electrodes showed remarkably reduced volume expansion, compared to the Al-Si. Presumably, Al$_2$O$_3$ protection layers with good mechanical properties and many void spaces in the foam can act as buffers for the large volume change of Si electrodes. To further characterize the stable structural integrity of the oxidized Si/Al$_2$O$_3$ particles, we measured SEM and TEM of the etched Al-Si and the Si/Al$_2$O$_3$ electrodes after 120 cycles. The etched Al-Si electrode showed a serious destruction of the original spherical shape particle due to a large volume change, while the oxidized sample retained the original shape with suppressed volume change (ESI, Fig. S10).

In summary, Si/Al$_2$O$_3$ foam particles were simply synthesized by the chemical etching of Al-Si alloy and a subsequent selective thermal oxidation process. The Si/Al$_2$O$_3$ electrodes with tunable Al$_2$O$_3$ thickness exhibited highly stable cycling performance, excellent rate capability, and suppressed volume expansion. This strategy opens up an effective way to introduce various protecting layers on the surface of other inorganic materials.

Acknowledgements

Notes and references

Department of Energy Engineering, School of Energy and Chemical Engineering, Ulsan National Institute of Science and Technology (UNIST), Ulsan 689-798, Korea. Tel: +82-52-217-2515
E-mail: spark@unist.ac.kr

1 H. Jung, *J. Power Sources*, 2003, **115**, 346-351.
2 U. Kasavajjula, C. Wang and A. J. Appleby, *J. Power Sources*, 2007, **163**, 1003-1039.
3 L. Hu, H. Wu, S. S. Hong, L. Cui, J. R. McDonough, S. Bohy and Y. Cui, *Chem. Commun.*, 2011, **47**, 367-369.
4 C. K. Chan, R. Ruffo, S. S. Hong, R. A. Huggins and Y. Cui, *J. Power Sources*, 2009, **189**, 34-39.
5 M.-H. Park, M. G. Kim, J. Joo, K. Kim, J. Kim, S. Ahn, Y. Cui and J. Cho, *Nano Lett.*, 2009, **9**, 3844-3847.
6 S. H. Ng, J. Wang, D. Wexler, S. Y. Chew and H. K. Liu, *J. Phys. Chem.*, 2007, **111**, 11131-11138.
7 C. K. Chan, H. Peng, G. Liu, K. McIlwrath, X. F. Zhang, R. A. Huggins and Y. Cui, *Nat. Nanotechnol.*, 2007, **3**, 31-35.
8 W. Zhou, T. Jiang, H. Zhou, Y. Wang, J. Fang and M. S. Whittingham, *MRS Commun.*, 2013, **3**, 119-121.
9 Z. Jiang, C. Li, S. Hao, K. Zhu and P. Zhang, *Electrochim. Acta*, 2014, **115**, 393-398.
10 M. Yoshio, H. Wang, K. Fukuda, T. Umeno, N. Dimov and Z. Ogumi, *J. Electrochem. Soc.*, 2002, **149**, A1598.
11 S. Yoo, J.-I. Lee, S. Ko and S. Park, *Nano Energy*, 2013, **2**, 1271-1278.
12 S. Sim, P. Oh, S. Park and J. Cho, *Adv. Mater.*, 2013, **25**, 4498-4503.
13 O. Park, J.-I. Lee, M.-J. Chun, J.-T. Yeon, S. Yoo, S. Choi, N.-S. Choi and S. Park, *RSC Adv.*, 2013, **3**, 2538.
14 H. Park, S. Lee, S. Yoo, M. Shin, J. Kim, M. Chun, N. S. Choi and S. Park, *ACS Appl. Mater. Interfaces*, 2014, **6**, 16360-16367.
15 Y. Yao, N. Liu, M. T. McDowell, M. Pasta and Y. Cui, *Energy Environ. Sci.*, 2012, **5**, 7927.
16 H. T. Nguyen, M. R. Zamfir, L. D. Duong, Y. H. Lee, P. Bondavalli and D. Pribat, *J. Mater. Chem.*, 2012, **22**, 24618.
17 Y. He, X. Yu, Y. Wang, H. Li and X. Huang, *Adv. Mater.*, 2011, **23**, 4938-4941.
18 A. M. Goodman and J. M. Breece, *J. Electrochem. Soc.*, 1970, **117**, 982-984.
19 J. Appenzeller, J. A. d. Alamo, R. Martel, K. Chan and P. Solomon, *Electrochem. Solid-State Lett.*, 2000, **3**, 84-86.
20 W. W. Smeltzer, *J. Electrochem. Soc.*, 1956, **103**, 209-214.
21 L. P. H. Jeurgens, W. G. Sloof, F. D. Tichelaar and E. J. Mittemeijer, *J. Appl. Phys.*, 2002, **92**, 1649.
22 Y. Hamon, T. Brousse, F. Jousse, P. Topart, P. Buvat and D. M. Schleich, *J. Power Sources*, 2001, **97-98**, 185-187.

ChemComm Accepted Manuscript